

Deep Image Feature Learning with Fuzzy Rules

Xiang Ma, Zhaohong Deng, *Senior Member, IEEE*, Peng Xu, Kup-Sze Choi, Shitong Wang

Abstract—The methods of extracting image features are the key to many image processing tasks. At present, the most popular method is the deep neural network which can automatically extract robust features through end-to-end training instead of hand-crafted feature extraction. However, the deep neural network currently faces many challenges: 1) its effectiveness is heavily dependent on large datasets, so the computational complexity is very high; 2) it is usually regarded as a black box model with poor interpretability. To meet the above challenges, a more interpretable and scalable feature learning method, i.e., deep image feature learning with fuzzy rules (DIFL-FR), is proposed in the paper, which combines the rule-based fuzzy modeling technique and the deep stacked learning strategy. The method progressively learns image features through a layer-by-layer manner based on fuzzy rules, so the feature learning process can be better explained by the generated rules. More importantly, the learning process of the method is only based on forward propagation without back propagation and iterative learning, which results in the high learning efficiency. In addition, the method is under the settings of unsupervised learning and can be easily extended to scenes of supervised and semi-supervised learning. Extensive experiments are conducted on image datasets of different scales. The results obviously show the effectiveness of the proposed method.

Index Terms—Stacked Learning; Representation Learning; TSK Fuzzy System; Image Processing

I. INTRODUCTION

IMAGE feature learning is the basic research content in the field of computer vision and machine learning, which is very important to meet with the requirements of practical applications and has been concerned by many researchers in related fields. The various tasks in computer vision, such as image classification, object detection, scene segmentation, etc., all treat the feature learning as the initial step through various feature learning methods, followed by other techniques to achieve their goals. The design and construction of image features not only affect the performance on the tasks, but also affect the feasibility and effectiveness of the models. In addition, it is non-trivial to design an effective method for image feature learning, since the robustness of learned features can be affected by various factors, such as occlusion, distortion and scaling. Therefore, it is important to devise an effective image representation method.

This work was supported in part by the National Key Research Pro-gram of China under Grant 2016YFB0800803, the NSFC under Grant 61772239, the Jiangsu Province Outstanding Youth Fund under Grant BK20140001, the National First-Class Discipline Program of Light Industry Technology and Engineering under Grant LITE2018-02, and Basic Research Program of Jiangnan University Key Project in Social Sciences JUSRP1810ZD. (Corresponding author: Zhaohong Deng)

At present, the methods to extract image features are mainly divided into two types: one is based on handcraft through feature extractors, and another is based on learning through machine learning or deep learning methods.

The handcraft-based methods can extract both global and local features. The global features usually contain all the information including the region of interest and the background. The most representative global feature extractors are HOG [1], LBP [2], color histograms, etc. The local features can flexibly describe the internal information and details of images. A series of methods based on the bag of words [3] has been proposed to extract the local features, such as soft quantization algorithm [4, 5], locality-constrained linear coding algorithm [6], spatial pyramid algorithm [7] and so on.

The learning-based methods can automatically get features without elaborately designed feature extractors. Compared with the handcraft-based methods, it can learn features directly from image data and can better reveal the intrinsic information of the data. Currently, the learning-based methods are mainly based on techniques of matrix decomposition and deep learning. The methods based on matrix decomposition is to find a mapping to transform high-dimensional image data into low-dimensional space and utilize the potential geometric structure information of the data. Researchers believe that high-dimensional image data is actually embedded in low-dimensional manifold in the high-dimensional space. Common matrix decomposition methods include vector quantization (VQ) [8], QR decomposition [9], singular value decomposition (SVD) [10], and nonnegative matrix factorization (NMF) [11]. Turk proposed the eigenface method [12], which applied principal component analysis (PCA) [13] to face recognition. Ronald proposed Fisherface [14], which used linear discriminant analysis (LDA) [15] to find the projection direction that maximizes the between-class scatter and minimizes the within-class scatter. The methods based on deep learning have received extensive attention in recent years. These methods extract more abstract and effective high-level information by combining low-level features to discover different feature representations of data [16]. Various deep learning models and structures has been proposed by researchers. Hinton et al. proposed deep belief networks (DBN) [17], which is a generative model that can extract high-level visual features of images. Christian et al. proposed convolutional neural networks (CNN) [18], which have the advantages of less network parameters and simplified

Xiang. Ma, Z. H. Deng, P. Xu, S. Wang are with the School of Digital Media, Jiangnan University and Jiangsu Key Laboratory of Digital Design and Software Technology, Wuxi 214122, China (e-mail: 6171610013@stu.jiangnan.edu.cn; dengzhaohong@jiangnan.edu.cn; 6171610015@stu.jiangnan.edu.cn; wxwangst@aliyun.com)

K.S. Choi is with The Centre for Smart Health, the Hong Kong Polytechnic University (e-mail: thomasks.choi@polyu.edu.hk)

training. One key factor for success of CNNs in image tasks is the use of convolutional architectures. To learn a filter bank in each stage of CNNs, a variety of techniques has been proposed, (e.g., regularized autoencoders or their variations [19]).

The handcraft and learning based methods have their distinctive advantages in various image processing tasks. However, they have some common defects, mainly in the following aspects: on the one hand, the handcraft-based methods tend to ignore the target object information in the image, and is too sensitive to target occlusion, distortion and scaling. Furthermore, image data has some characteristics such as huge data volume, high dimension, unstructured data shape, and uncertainty. These characteristics make the handcraft-based methods not only time-consuming and laborious, but also difficult to design and extract features. Hence, it cannot be directly applied to high-dimensional image analysis and processing [19]. On the other hand, the learning-based methods, such as the DNNs, have strong hypothesis space and need to be driven by a large size of data. When the amount of data is small, neural networks often fail to achieve satisfactory performance and are easy to fall into the local optimum, which leads to poor generalization ability of the model. In addition, neural networks usually need to use the back propagation [20] algorithm to train. When the number of network layers is large, the vanishing gradient problem occurs, which leads to a long training time to convergence for the model. In general, such a network are typically learned by stochastic gradient descent (SGD) [21] method. However, the performance of the resulting model seriously depends on expertise of parameter tuning and some ad hoc tricks. In particular, neural networks are generally considered to be a black box model with poor interpretability.

In order to overcome the above drawbacks of the existing image feature methods, this paper proposes the deep image feature learning with fuzzy rules (DIFL-FR). This method effectively combines the interpretability advantages of rule-based fuzzy systems and layer-wise features extraction of deep learning. Specifically, the rule-based TSK fuzzy system (TSK-FS) [22–24] is firstly taken as a feature learning model, which is intuitive and easy to interpret. Then, the parameters of TSK-FS are optimized by specific feature learning objective so as to obtain the feature extraction model that can be interpreted by rules. Further, by means of layer-wise learning, image features are extracted layer by layer.

DIFL-FR has the following advantages. Firstly, compared with the handcraft-based methods, DIFL-FR can automatically learn features from the data. Secondly, compared with DNN, the training of DIFL-FR does not rely on large-scale data, and the results show the effectiveness on the datasets with different scales. Thirdly, DIFL-FR is based on rules and fuzzy inference to achieve feature extraction, so the process of feature extraction has better interpretability.

The main contributions of the paper are summarized as follows:

1) Different from the classic TSK-FS, which is usually used for classification and regression tasks, TSK-FS is regarded as a feature extraction model for image feature extraction in this paper. And then a novel deep image learning method based on

fuzzy rules (DIFL-FR) is proposed.

2) By using the stack structure and sliding window strategy of deep learning, a deep TSK-FS image feature learning method with layer-wise image feature extraction capability is proposed.

3) Extensive experiments are conducted on the image datasets with different scales. The experimental results obviously show the effectiveness and superiority of the proposed method.

The remainder of this paper is organized as follows. The related work of the proposed method is given in Section II, including the fundamentals of convolutional neural network and TSK-FS. The details of the proposed method are illustrated in Section III. In Section IV, the experimental results and the analysis are given. Finally, the conclusions are presented in Section V.

II. RELATED WORK

The relevant knowledge of convolutional neural networks for image feature learning are reviewed first in this section. And then the fundamentals of the TSK FS are described briefly.

A. Convolution Neural Network

Deep learning methods are good at extracting abstract feature representations from raw data, which have hierarchical structures that includes multi-layer nonlinear transformations. As one of the classic deep learning models, convolutional neural networks (CNNs) [17, 25–27] have been the most widely used structures in the field of image processing. Local receptive field, shared weights and pooling in CNNs can reduce the complexity of the network. CNNs are non-sensitive to the occlusion, distortion and scaling to some extent, which results in its robustness and fault tolerance.

CNNs are mainly composed of convolutional layers, pooling layers and fully connected layers. The convolutional layer is the core of the convolutional neural network. It imitates the mechanism of local receptive field. The convolutional operation is widely used in the field of image processing. Different convolutional kernels can extract different features such as edges, textures or corners, etc. In deep convolutional neural networks, different types of features, from simple to complex, can be extracted by different convolutional operations from the original image. In general, the outputs of the convolutional layer will be activated by the nonlinear functions and then the feature maps are formed by the activated results. The commonly used activation functions contain the sigmoid function and the ReLU function that has been widely used in recent years. The pooling layer, also called the subsampling layer, conducts the partial down-sampling on the feature maps of the former layer. The commonly used manners contain maximum pooling and average pooling. Through the pooling operation, the complexity of the model can be compressed, which also results in the non-sensitivity to the translation and rotation of the images. The fully connected layer is equivalent to the hidden layer in a traditional feedforward neural network. It is usually built at the end of the CNN. The purpose of the fully connected layer is to map the features learned by the network into the label space of the samples. In some CNNs, the

function of the full connection layer can be partially replaced by global average pooling [28].

B. TSK Fuzzy System

Fuzzy System [29] is a model based on fuzzy rules and fuzzy logic. By using fuzzy sets [30] and fuzzy membership functions, fuzzy system can directly transform human natural semantics into machine languages that can be recognized by computers. Fuzzy system is increasingly being applied to various fields of artificial intelligence due to its powerful learning ability and good interpretability, such as pattern recognition, intelligent control, data mining, image processing and so on. TSK FS [29, 31] is one of the most popular fuzzy system models. We will explore the image feature learning based on the TSK FS in this paper, which is described as follows.

TSK FS contains a fuzzy rule base, in which the k -th fuzzy rule can be formulated as follows:

$$\begin{aligned} R^k: & \text{ IF } x_1 \text{ is } A_1^k \wedge x_2 \text{ is } A_2^k \wedge \dots \wedge x_d \text{ is } A_d^k, \\ & \text{ THEN } f^k(\mathbf{x}) = p_0^k + p_1^k x_1 + \dots + p_d^k x_d, \end{aligned} \quad (2.1)$$

$k = 1, 2, \dots, K$

where $\mathbf{x} = [x_1, x_2, \dots, x_d]^T$ is an input vector, A_i^k is the fuzzy set [32] for the i -th feature in the k -th rule, and \wedge denotes the fuzzy conjunction operator. The final output can be calculated as follows:

$$y = \sum_{k=1}^K \frac{\mu^k(\mathbf{x})}{\sum_{k'}^K \mu^{k'}(\mathbf{x})} f^k(\mathbf{x}) = \sum_{k=1}^K \tilde{\mu}^k(\mathbf{x}) f^k(\mathbf{x}) \quad (2.2a)$$

where:

$$\mu^k(\mathbf{x}) = \prod_{i=1}^d \mu_{A_i^k}(x_i) \quad (2.2b)$$

$$\tilde{\mu}^k(\mathbf{x}) = \mu^k(\mathbf{x}) / \sum_{k'=1}^K \mu^{k'}(\mathbf{x}) \quad (2.2c)$$

where $\mu_{A_i^k}(x_i)$ is the membership of the x_i to fuzzy set A_i^k .

If the multiplication is used as the conjunction operator, the firing level of the k -th rule of each sample can be formulated as (2.2b) and its normalized form as that in (2.2c). The Gaussian membership function is used in this paper:

$$\mu_{A_i^k}(x_i) = \exp\left(\frac{-(x_i - c_i^k)^2}{2\delta_i^k}\right) \quad (2.2d)$$

where c_i^k , δ_i^k in (2.2d) are called antecedent parameters and can be estimated using different approaches, e.g., fuzzy c-means clustering algorithm [33] and deterministic clustering algorithm [34].

Once the antecedent parameters are obtained, TSK-FS can be represented as a linear model in a new feature space. The details are explained as follows. Let:

$$\mathbf{x}_e = (1, \mathbf{x}^T)^T \quad (2.3a)$$

$$\tilde{\mathbf{x}}^k = \tilde{\mu}^k(\mathbf{x}) \mathbf{x}_e \quad (2.3b)$$

$$\mathbf{x}_g = \left[(\tilde{\mathbf{x}}^1)^T, (\tilde{\mathbf{x}}^2)^T, \dots, (\tilde{\mathbf{x}}^K)^T \right]^T \quad (2.3c)$$

$$\mathbf{p}^k = (p_0^k, p_1^k, \dots, p_d^k)^T \quad (2.3d)$$

$$\mathbf{p}_g = \left[(\mathbf{p}^1)^T, (\mathbf{p}^2)^T, \dots, (\mathbf{p}^K)^T \right]^T \quad (2.3e)$$

Then, the output of TSK-FS in (2.2a) can be re-expressed in (2.3f)

$$y = \mathbf{p}_g^T \mathbf{x}_g \quad (2.3f)$$

where, $\mathbf{x}_g \in R^{K(d+1) \times 1}$ represents the feature vector in the new feature space that is transformed from the original input vector $\mathbf{x} \in R^{d \times 1}$. \mathbf{p}_g is the combination of the consequent parameters of all fuzzy rules.

Remark: TSK-FS has been widely used in classification and regression tasks. Using labeled datasets and supervised learning methods to train the TSK-FS system, the interpretable discriminative model based on rules can be obtained. Different from the construction of the classification and regression models by using the classic TSK-FS, in this paper, TSK-FS is used for feature extraction tasks in order to implement interpretable image feature extraction based on rules.

III. DEEP IMAGE FEATURE LEARNING WITH FUZZY RULES

This section proposes DIFL-FR, a novel deep image feature learning method based on fuzzy rules. The model is a cascaded structure consisting of basic components, i.e., multi-layer TSK-FS image feature learning, weight binarization, and block-wise histograms. The proposed method realizes nonlinear transformation by the antecedent part of the multi-output TSK-FS to generate hidden features. The transformation of the hidden feature space provides a nonlinear feature learning ability like the activation functions in the classic CNNs, while also having good interpretability. DIFL-FR generates different new features through multiple-group consequent parameters which is similar to the convolution kernels in CNNs. The multi-layer TSK-FS image feature learning can extract deeper image features in a progressive way.

The rationales of proposed DIFL-FR are described through five parts as follows. The overall structure of DIFL-FR is shown in Section III-A. The first and s -th layers of TSK-FS image feature learning are presented in Section III-B and Section III-C respectively. The details of the output layer are given in Section III-D.

A. The Architecture of Deep Image Feature Learning based on Fuzzy Rules

The proposed DIFL-FR is an end-to-end learning method that automatically learns features from raw data without handcraft. DIFL-FR consists of two parts, i.e., the multi-layer TSK-FS image feature learning and a feature output layer respectively. The architecture of DIFL-FR with two layers TSK-FS image feature learning is illustrated in Fig. 1.

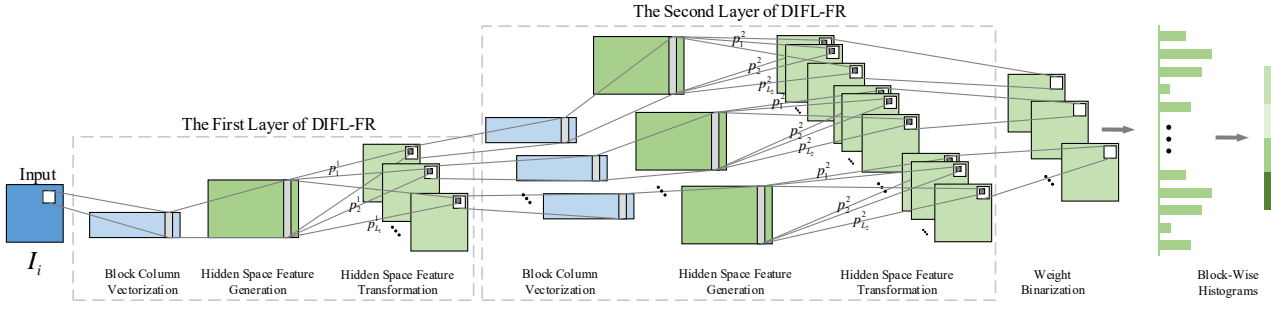


Fig. 1. The architecture of the proposed method (DIFL-FR)

B. The First Layer of DIFL-FR

The feature space construction is fundamental in feature learning. TSK-FS image feature learning consists of three steps: patch sliding process, feature generation in the hidden space, and feature transformation in the hidden space. Fig. S1 in Part A of the *Supplementary Martials* section shows the process of the TSK-FS image feature learning. Firstly, TSK-FS image feature learning scans the original input image and vectorizes it. Secondly, a non-linear transformation is implemented by the antecedent part of the multi-output TSK-FS to generate a hidden feature space. Thirdly, the feature dimensional reduction is achieved by linear transformation of hidden space through the consequent part of multi-output TSK-FS. The more detailed descriptions are as follows.

Let us denote the number of input training image as N , then, the image dataset can be represented as $\{\mathbf{I}_i\}_{i=1}^N$, the size of each image as $m \times n$. Let the N images be concatenated as a matrix $\mathbf{I} = [\mathbf{I}_1, \mathbf{I}_2, \dots, \mathbf{I}_N]$.

1) Block Column Vectorization

For the input image \mathbf{I}_i of size $m \times n$, considering that the spatial relationship of images holds the characteristic of close local pixel connections, this paper uses a patch of size $h_1 \times h_2$ to scan each pixel of the image \mathbf{I}_i (the edges of the image are filled with 0) and then reshape each $h_1 \times h_2$ matrix into a column vector (as shown in Fig. S2 in Part A of the *Supplementary Martials* section). Then the vector corresponding to the image \mathbf{I}_i can be represented as (3.1).

$$\mathbf{X}_i = [\mathbf{x}_{i,1}, \mathbf{x}_{i,2}, \dots, \mathbf{x}_{i,mn}] \in R^{h_1 h_2 \times mn}, i = 1, 2, \dots, N \quad (3.1)$$

where $\mathbf{x}_{i,j} \in R^{h_1 h_2 \times 1}$ denotes the j -th vectorized patch in \mathbf{I}_i .

Therefore, for all the input training images $\{\mathbf{I}_i\}_{i=1}^N$, the vector set can be represented as (3.2).

$$\mathbf{X} = [\mathbf{X}_1, \mathbf{X}_2, \dots, \mathbf{X}_N] \in R^{h_1 h_2 \times mnN} \quad (3.2)$$

2) Hidden Space Feature Generation

Based on the principle of TSK-FS, the fuzzy membership in the antecedent part of fuzzy rules can be generated according to (2.2a)-(2.2d). Fuzzy c-means (FCM) is a common method to obtain the antecedent parameters of TSK-FS, but its stability is poor due to the random initialization of FCM. Therefore, in the proposed method DIFL-FR, a deterministic clustering

algorithm Var-Part is adopted to obtain the antecedent parameters. For the details of Var-Part, please see Part B of the *Supplementary Martials* section.

Once the fuzzy membership is known, according to (2.3a)-(2.3c), the original features can be mapped from the original feature space \mathbf{X} to the hidden feature space, and the dataset \mathbf{G} of the new hidden feature space is obtained.

$$\mathbf{G} = [\mathbf{G}_1, \mathbf{G}_2, \dots, \mathbf{G}_N] \in R^{K(h_1 h_2 + 1) \times mnN} \quad (3.3a)$$

$$\begin{aligned} \mathbf{G}_i &= [\mathbf{g}_{i,1}, \mathbf{g}_{i,2}, \dots, \mathbf{g}_{i,mn}] \\ &= [\mathbf{x}_{gi,1}, \mathbf{x}_{gi,2}, \dots, \mathbf{x}_{gi,mn}] \in R^{K(h_1 h_2 + 1) \times mn} \end{aligned} \quad (3.3b)$$

$$\begin{aligned} \mathbf{g}_{i,j} &= \mathbf{x}_{gi,j} \\ &= \left[(\tilde{\mathbf{x}}_{i,j}^1)^T, (\tilde{\mathbf{x}}_{i,j}^2)^T, \dots, (\tilde{\mathbf{x}}_{i,j}^K)^T \right]^T \in R^{K(h_1 h_2 + 1) \times 1} \end{aligned} \quad (3.3c)$$

where \mathbf{G} is the concatenated data of \mathbf{G}_i for all images in the dataset after all the images are converted into \mathbf{G}_i . \mathbf{G}_i is the matrix concatenated by $\mathbf{g}_{i,j}$ ($\mathbf{g}_{i,j} = \mathbf{x}_{gi,j}$) that is defined by (2.3a)-(2.3c). $\mathbf{g}_{i,j}$ is a vector that maps from the original feature space to the new hidden feature space through the antecedent part of fuzzy rules, as shown in Fig. S3 in Part A of the *Supplementary Martials* section.

3) Hidden Space Feature Transformation

If the data transformed by the antecedent part of the multi-output TSK-FS is viewed as a hidden feature representation in the high-dimensional space, the consequent part of the multi-output TSK-FS can be viewed as a linear dimensional reduction of the hidden feature representation space. In order to preserve the geometric properties of the data during dimensional reduction, the PCA is used by maximizing the variance for the data in the hidden feature space to optimize the consequent parameters \mathbf{P} of TSK-FS. The optimization objective of consequent parameters \mathbf{P} can be formulized as follows:

$$\max_{\mathbf{P}} \text{Tr}(\mathbf{P}^T \overline{\mathbf{G}} \mathbf{G}^T \mathbf{P}), \text{ s.t. } \mathbf{P}^T \mathbf{P} = \mathbf{I}_{L_1} \quad (3.4a)$$

where $\overline{\mathbf{G}}$ is the matrix obtained by centralizing the hidden feature space data \mathbf{G} , \mathbf{I}_{L_1} is an identity matrix of size $L_1 \times L_1$. Specifically, for each input training image \mathbf{I}_i , the following centralization matrix can be obtained:

$$\overline{\mathbf{G}}_i = [\overline{\mathbf{g}}_{i,1}, \overline{\mathbf{g}}_{i,2}, \dots, \overline{\mathbf{g}}_{i,mn}] \in R^{K(h_1 h_2 + 1) \times mn} \quad (3.4b)$$

where $\overline{\mathbf{g}}_{i,j}$ is a mean-removed vector.

Thus, for all the training images $\{\mathbf{I}_i\}_{i=1}^N$, the centralization matrix of the dataset can be obtained by $\overline{\mathbf{G}} = [\overline{\mathbf{G}}_1, \overline{\mathbf{G}}_2, \dots, \overline{\mathbf{G}}_N] \in R^{K(h_1 h_2 + 1) \times mnN}$. The Lagrange multiplier method is used to optimize (3.4a).

$$\overline{\mathbf{G}} \overline{\mathbf{G}}^T \mathbf{p}_g^i = \lambda_i^1 \mathbf{p}_g^i \quad (3.5a)$$

Therefore, the optimization problem in (3.4a) is transformed into the following problem of eigenvalue decomposition:

$$\mathbf{C}_1 = \mathbf{P} \mathbf{\Lambda}_1 \mathbf{P}^T \quad (3.5b)$$

with

$$\mathbf{C}_1 = \frac{1}{mnN} \overline{\mathbf{G}} \overline{\mathbf{G}}^T \in R^{K(h_1 h_2 + 1) \times K(h_1 h_2 + 1)} \quad (3.5c)$$

$\mathbf{\Lambda}_1$ is a diagonal matrix composed of the first L_1 largest eigenvalues of \mathbf{C}_1 , i.e.,

$$\mathbf{\Lambda}_1 = \text{diag}(\lambda_1^1), l_1 = 1, 2, \dots, L_1 \quad (3.5d)$$

where $\lambda_1^1 \geq \lambda_2^1 \geq \dots \geq \lambda_{L_1}^1$. \mathbf{P} is the matrix composed of the corresponding eigenvectors as follows:

$$\mathbf{P} = [\mathbf{p}_g^1, \mathbf{p}_g^2, \dots, \mathbf{p}_g^{L_1}] \in R^{K(h_1 h_2 + 1) \times L_1} \quad (3.5e)$$

where $\mathbf{p}_g^{l_1}$ represents the l_1 -th eigenvector, that is, the consequent parameters corresponding to the l_1 -th output of the multi-output TSK-FS.

Once the consequent parameters \mathbf{P} are determined, the new feature data learned by TSK-FS can be obtained easily.

$$\mathbf{Z}^1 = \mathbf{P}^T \overline{\mathbf{G}} \quad (3.6a)$$

$$\mathbf{Z}^1 = [\mathbf{Z}_1^1; \mathbf{Z}_2^1; \dots; \mathbf{Z}_{L_1}^1] \quad (3.6b)$$

$$\mathbf{Z}_{l_1}^1 = [\mathbf{z}_{i,l_1}^1, \mathbf{z}_{2,l_1}^1, \dots, \mathbf{z}_{N,l_1}^1], l_1 = 1, 2, \dots, L_1 \quad (3.6c)$$

$$\mathbf{z}_{i,l_1}^1 = [z_{i,l_1,1}^1, z_{i,l_1,2}^1, \dots, z_{i,l_1,mn}^1], i = 1, 2, \dots, N \quad (3.6d)$$

$$z_{i,l_1,j}^1 = (\mathbf{p}_g^{l_1})^T \overline{\mathbf{g}}_{i,j}, i = 1, 2, \dots, N; \quad (3.6e)$$

$$l_1 = 1, 2, \dots, L_1; j = 1, 2, \dots, mn$$

Here, $z_{i,l_1,j}^1$ is the result of the j -th block in the i th image, which is obtained by the l_1 -th group of consequent parameters. It represents the features of each block. For each training image \mathbf{I}_i , the number of results obtained by the l_1 -th group of consequent parameters is mn . These results can be reconstructed into an image of the same size as the original training image. There are L_1 groups of consequent parameters in the first layer, so that each image has L_1 new feature images. Thus, the feature image of the first layer is formed as (3.7).

$$\mathbf{I}_{i,l_1}^1 \in R^{mn \times n}, l_1 = 1, 2, \dots, L_1 \quad (3.7)$$

For all input training images $\{\mathbf{I}_i\}_{i=1}^N$, the matrix corresponding to the set of feature images can be expressed as follows:

$$\mathbf{I}^1 = [\mathbf{I}_{1,1}^1, \mathbf{I}_{1,2}^1, \dots, \mathbf{I}_{1,L_1}^1, \dots, \mathbf{I}_{N,1}^1, \mathbf{I}_{N,2}^1, \dots, \mathbf{I}_{N,L_1}^1] \quad (3.8)$$

Besides the PCA feature transformation criteria defined in (3.4a), other more complicated criteria can be also used to optimize the consequent parameters \mathbf{P} . The PCA optimization

criteria adopted in this paper is only a viable option.

C. The s -th Layer of DIFL-FR

The process of constructing the s -th ($s \geq 2$) layer of DIFL-FR are basically the same as those of the first layer of DIFL-FR. The steps are briefly described below.

1) Block column vectorization

Refer to the steps of block column vectorization in the first layer, and use the output of the $(s-1)$ -th layer for the input of the s -th layer. Similarly, for the input feature image $\mathbf{I}_{i,\ell_{s-1}}^{s-1}$, $i = 1, 2, \dots, N$, $\ell_{s-1} = 1, 2, \dots, \Gamma_{s-1}$, $\Gamma_{s-1} = \prod_{n=s-1}^{s-1} L_{n-s}$, each pixel point takes a patch of size $h_1 \times h_2$, and the information of all points is concatenated through block vectorization to obtain (3.9).

$$\mathbf{X}_{i,\ell_{s-1}}^s = [\mathbf{x}_{i,\ell_{s-1},1}^s, \mathbf{x}_{i,\ell_{s-1},2}^s, \dots, \mathbf{x}_{i,\ell_{s-1},mn}^s] \in R^{h_1 h_2 \times mn} \quad (3.9)$$

where $\mathbf{I}_{i,\ell_{s-1}}^{s-1}$ represents the ℓ_{s-1} -th feature image of the i th original image obtained through the first $s-1$ layer TSK-FS image feature learning. $\mathbf{x}_{i,\ell_{s-1},j}^s \in R^{h_1 h_2 \times 1}$ represents the column vector of the j -th block in $\mathbf{I}_{i,\ell_{s-1}}^{s-1}$. Therefore, for each input training image \mathbf{I}_i , it can be represented as (3.10).

$$\mathbf{X}_i^s = [\mathbf{X}_{i,1}^s, \mathbf{X}_{i,2}^s, \dots, \mathbf{X}_{i,\Gamma_{s-1}}^s] \in R^{h_1 h_2 \times \Gamma_{s-1} mn} \quad (3.10)$$

For all the input training images $\{\mathbf{I}_i\}_{i=1}^N$, the matrix can be concatenated as (3.11).

$$\mathbf{X}^s = [\mathbf{X}_1^s, \mathbf{X}_2^s, \dots, \mathbf{X}_N^s] \in R^{h_1 h_2 \times \Gamma_{s-1} mnN} \quad (3.11)$$

2) Hidden Space Feature Generation

Similar to the hidden space feature generation method in the first layer of DIFL-FR, the feature matrix \mathbf{X}^s can be mapped to the new hidden feature space matrix \mathbf{G}^s , that is, the new feature space spanned by the antecedent part of rules. Then the matrix (3.12) can be obtained. K_s represents the number of rules for the s -th layer TSK-FS image feature learning.

$$\mathbf{G}^s = [\mathbf{G}_1^s, \mathbf{G}_2^s, \dots, \mathbf{G}_N^s] \in R^{K_s (h_1 h_2 + 1) \times \Gamma_{s-1} mnN} \quad (3.12)$$

3) Hidden Space Feature Transformation

By centralizing the hidden space \mathbf{G}^s , (3.13a) can be obtained as follows:

$$\overline{\mathbf{G}}^s = [\overline{\mathbf{G}}_1^s, \overline{\mathbf{G}}_2^s, \dots, \overline{\mathbf{G}}_N^s] \in R^{K_s (h_1 h_2 + 1) \times \Gamma_{s-1} mnN}, \quad (3.13a)$$

$$\Gamma_{s-1} = \prod_{n=s-1}^{s-1} L_{n-s}$$

$$\overline{\mathbf{G}}_i^s = [\overline{\mathbf{g}}_{i,1}^s, \overline{\mathbf{g}}_{i,2}^s, \dots, \overline{\mathbf{g}}_{i,\Gamma_{s-1}}^s] \in R^{K_s (h_1 h_2 + 1) \times \Gamma_{s-1} mn}, \quad (3.13b)$$

$$i = 1, 2, \dots, N$$

$$\overline{\mathbf{G}}_{i,\ell_{s-1}}^s = [\overline{\mathbf{g}}_{i,\ell_{s-1},1}^s, \overline{\mathbf{g}}_{i,\ell_{s-1},2}^s, \dots, \overline{\mathbf{g}}_{i,\ell_{s-1},mn}^s] \in R^{K_s (h_1 h_2 + 1) \times mn}, \quad (3.13c)$$

$$\ell_{s-1} = 1, 2, \dots, \Gamma_{s-1}$$

where $\overline{\mathbf{g}}_{i,\ell_{s-1},j}^s$ is a mean-removed vector.

As with the first layer of DIFL-FR, the PCA optimization criterion is used to solve the consequent parameters $\mathbf{P}^s = [\mathbf{p}_g^{s,1}, \mathbf{p}_g^{s,2}, \dots, \mathbf{p}_g^{s,L_s}] \in R^{K_s (h_1 h_2 + 1) \times L_s}$ of the s -th layer of

DIFL-FR. Here $\mathbf{p}_g^{s,l}$ represents the consequent parameter corresponding to the l_s -th output of the multi-output TSK-FS.

Once the consequent parameters \mathbf{P}^s are determined, the new feature learned by the s -th layer of DIFL-FR can be obtained:

$$\mathbf{Z}^s = (\mathbf{P}^s)^T \overline{\mathbf{G}}^s \quad (3.14a)$$

$$\mathbf{Z}^s = [\mathbf{Z}_1^s; \mathbf{Z}_2^s; \dots; \mathbf{Z}_{L_s}^s] \quad (3.14b)$$

$$\mathbf{Z}_{l_s}^s = [\mathbf{Z}_{1,l_s}^s; \mathbf{Z}_{2,l_s}^s; \dots; \mathbf{Z}_{N,l_s}^s], \quad l_s = 1, 2, \dots, L_s \quad (3.14c)$$

$$\mathbf{Z}_{i,l_s}^s = [z_{i,l_s,1}^s; z_{i,l_s,2}^s; \dots; z_{i,l_s,\Gamma_{s-1}}^s], \quad (3.14d)$$

$$i = 1, 2, \dots, N, \quad \Gamma_{s-1} = \prod_{n=s-1}^s L_{n-s}$$

$$\mathbf{z}_{i,l_s,\ell_{s-1}}^s = [z_{i,l_s,\ell_{s-1},1}^s; z_{i,l_s,\ell_{s-1},2}^s; \dots; z_{i,l_s,\ell_{s-1},mn}^s], \quad (3.14e)$$

$$\ell_{s-1} = 1, 2, \dots, \Gamma_{s-1}$$

$$z_{i,l_s,\ell_{s-1},j}^s = (\mathbf{p}_g^{s,l_s})^T \mathbf{g}_{i,l_s,\ell_{s-1},j}^s, \quad j = 1, 2, \dots, mn \quad (3.14f)$$

where $z_{i,l_s,\ell_{s-1},j}^s$ represents the new feature of the j -th block in the ℓ_{s-1} -th feature image $\mathbf{I}_{i,\ell_{s-1}}^{s-1}$, which is obtained by the l_s -th group of consequent parameters of the s -th layer TSK-FS. $\mathbf{I}_{i,\ell_{s-1}}^{s-1}$ represents the ℓ_{s-1} -th feature image obtained after the i th original image is learned by the first $s-1$ layer TSK-FS image feature learning. For each input feature image $\mathbf{I}_{i,\ell_{s-1}}^{s-1}$, a total of mn new feature values $z_{i,l_s,\ell_{s-1},j}^s$ can be obtained. These results can be reconstructed into an image of the same size as the original training image. Thus, the feature image $\mathbf{I}_{i,l_s,\ell_{s-1}}^s$ is formed. There are L_s groups of consequent parameters in the s -th layer, so that each input feature image $\mathbf{I}_{i,\ell_{s-1}}^{s-1}$ can generate L_s new feature images $\{\mathbf{I}_{i,l_s,\ell_{s-1}}^s, l_s = 1, 2, \dots, L_s\}$. For each original image, a total of Γ_s ($\Gamma_s = \prod_{n=s-1}^s L_{n-s}$) feature image can be obtained. Therefore, for all input training images $\{\mathbf{I}_i\}_{i=1}^N$, after the s -layer TSK-FS image feature learning, the feature image set can be represented as follows:

$$\{\mathbf{I}_{i,\ell_s}^s \in R^{m \times n}\}, \quad i = 1, 2, \dots, N; \ell_s = 1, 2, \dots, \Gamma_s; \Gamma_s = \prod_{n=s-1}^s L_{n-s}$$

The above feature image set \mathbf{I}^s can be represented as the following matrix form:

$$\mathbf{I}^s = [\mathbf{I}_{1,1}^s; \mathbf{I}_{1,2}^s; \dots; \mathbf{I}_{1,\Gamma_s}^s; \dots; \mathbf{I}_{N,1}^s; \mathbf{I}_{N,2}^s; \dots; \mathbf{I}_{N,\Gamma_s}^s], \quad (3.15)$$

$$\Gamma_s = \prod_{n=s-1}^s L_{n-s}$$

D. Output Layer

The output layer of DIFL-FR first performs weight binarization on the feature image extracted by the previous multiple cascaded TSK-FSs, and then converts it into a block histogram statistical vector as the final features extracted by the model.

1) Weight Binarization

The output layer first binarizes the feature image obtained by the s -th layer, and the binarization function is defined as follows:

$$\mathbf{P}_{i,l_s,\ell_{s-1}} = H(\mathbf{I}_{i,l_s,\ell_{s-1}}^s), \quad i = 1, 2, \dots, N; \quad (3.16)$$

$$l_s = 1, 2, \dots, L_s; \ell_{s-1} = 1, 2, \dots, \Gamma_{s-1}$$

where $H(x) = \begin{cases} 1, & x \geq 0 \\ 0, & x < 0 \end{cases}$ is a Heaviside step function.

For the L_s binary images generated by the ℓ_{s-1} -th feature image, the value of each pixel at the same position is regarded as one of the L_s -bit binary numbers. Thus, these L_s binary images can be converted into an integer-valued feature image, which is denoted as $\mathbf{T}_{i,\ell_{s-1}}$. $\mathbf{T}_{i,\ell_{s-1}}$ represents an integer-valued feature image generated by the ℓ_{s-1} -th feature image, which is obtained from the i th original input image in the s -th layer. Every pixel in $\mathbf{T}_{i,\ell_{s-1}}$ is an integer in the range $[0, 2^{L_s} - 1]$.

$$\mathbf{T}_{i,\ell_{s-1}} = \sum_{l_s=1}^{L_s} 2^{l_s-1} \mathbf{P}_{i,l_s,\ell_{s-1}} \quad (3.17)$$

All integer-valued feature images corresponding to all training images can be expressed as the following matrix:

$$\mathbf{T} = [\mathbf{T}_{1,1}; \mathbf{T}_{1,2}; \dots; \mathbf{T}_{1,\Gamma_{s-1}}; \dots; \mathbf{T}_{N,1}; \mathbf{T}_{N,2}; \dots; \mathbf{T}_{N,\Gamma_{s-1}}].$$

2) Block-wise Histograms

This paper use a block of size $h_1 \times h_2$ to slide the integer-valued feature image $\mathbf{T}_{i,\ell_{s-1}}$ with overlap ratio Cr (default is 0.5, that is, step size is $\lfloor h_1 / 2 \rfloor, \lfloor h_2 / 2 \rfloor$), and partition $\mathbf{T}_{i,\ell_{s-1}}$ into B blocks. For each block, the histogram (in the range $[0, 2^{L_s} - 1]$) of the decimal values can be computed, and the output of each block is a 2^{L_s} -dimensional vector. For $\mathbf{T}_{i,\ell_{s-1}}$, there are a total of B block, and these 2^{L_s} -dimensional vectors can be concatenated into a vector, expressed as $\mathbf{h}_{i,\ell_{s-1}} = \text{Hist}(\mathbf{T}_{i,\ell_{s-1}}) \in R^{(2^{L_s})^{\Gamma_{s-1} \times 1}}$, where $\text{Hist}()$ is the operator that uses the block histogram statistics and expands the result as a vector.

For an original input image, after k -layer image feature learning based on TSK-FS, weight binarization and block-wise histogram operations, the output feature vector can be expressed as

$$\mathbf{f}_i = [\mathbf{h}_{i,1}; \mathbf{h}_{i,2}; \dots; \mathbf{h}_{i,\Gamma_{s-1}}] \in R^{(2^{L_s})^{\Gamma_{s-1} B \times 1}}, \quad (3.18)$$

$$\Gamma_{s-1} = \prod_{n=s-1}^s L_{n-s}$$

Therefore, the original image dataset $\{\mathbf{I}_i\}_{i=1}^N$ can be transformed into the feature matrix (3.19).

$$\mathbf{F} = [\mathbf{f}_1; \mathbf{f}_2; \dots; \mathbf{f}_N] \in R^{(2^{L_s})^{\Gamma_{s-1} B \times N}}, \Gamma_{s-1} = \prod_{n=s-1}^s L_{n-s} \quad (3.19)$$

Finally, the extracted features can be put into a common classifier for learning.

For the details of multi-output TSK-FS, please see Part C of the *Supplementary Materials* section. Table S1 in the part D of the *Supplementary Materials* section gives a specific algorithm description of the proposed DIFL-FR method.

IV. EXPERIMENTS

The extensive experiments are conducted to evaluate the effectiveness of the proposed image extraction method DIFL-FR. Specifically, the performance of the proposed method on small-scale and larger-scale image datasets is discussed. In this section, DIFL-FR with two layers is selected for experiments. If there is no specific description of layers, DIFL-FR with two layers is selected for experiments in this section.

In order to evaluate the classification performance, a classifier is required that is trained based on the extracted image features, and then the classification accuracy is used as the indicator to evaluate the performance. In our experiments, the multi-class linear SVM [35] is selected as the classifier.

A. Small-scale datasets

In this section, the proposed method DIFL-FR is evaluated on two small-scale face recognition datasets [36–38], i.e., ORL dataset and Extended Yale B dataset.

In the experiments, two handcraft-based methods and three learning-based methods with matrix decomposition are used as the comparative algorithms. Due to the small size of the adopted datasets, DNNs perform poorly on them, and therefore the algorithms related with DNNs are not included for comparison in this section. Meanwhile, the original image is treated as the benchmark algorithm (represented as Raw), where the original pixels of the image are directly used for the classifier without feature extraction. Two handcraft-based methods are block histogram (BlockHist) and local binary pattern (LBP) respectively. Three learning-based methods are principal component analysis (PCA), kernel principal component analysis (KPCA) and Fisherface respectively.

The five-fold cross-validation is adopted to search the optimal settings of the parameters for all comparative algorithms, and the maximum mean accuracy is reported.

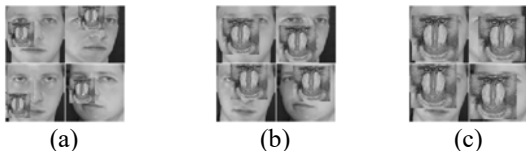


Fig. 3. Test face image with various levels of occlusion on the ORL dataset: (a)20% Occlusion. (b)40% Occlusion. (c)80% Occlusion.

For BlockHist, the overlap ratio Cr is set as 0.5, and the block size is optimally set by searching grid $h=\{3,5,7,9,11\}$.

For LBP, the image is equally divided into 4×4 sub-areas. In each sub-area, the histogram is counted using the uniform LBP, and then the obtained statistical histogram of each sub-area is concatenated as one feature vector. For PCA and KPCA, the dimension of subspace is optimally set by searching grid $m=\{10,12,14,\dots,400\}$. The kernel type of KPCA selects the Gaussian kernel, and the parameters of the Gaussian kernel are optimally set by searching grid $t=\{2^{-4},2^{-3},\dots,2^4\}$. For Fisherface, the dimension of subspace is fixed to the number of categories -1.

For the proposed method DIFL-FR, the block size of each pixel is set as 5×5 , the overlap ratio Cr in the output layer is set as 0.5. For DIFL-FR with two layers of TSK-FS, the two important parameters are the number of rules for each layer and the number of groups for calculating the consequent parameters in each feature learning phase. They are optimally set by searching grid $K_1, K_2 = \{2, 3, \dots, 10\}$ and $L_1, L_2 = \{4, 5, \dots, 16\}$.

In order to comprehensively verify that DIFL-FR can achieve good performance when the amount of training data is small, the training set and test set are divided into different proportions, and the details of datasets are shown in Part E of the *Supplementary Materials* section

1) ORL Database

The ORL face dataset consists of 400 face images taken by the AT&T Lab from April 1992 to April 1994, with a total of 40 distinct subjects. All the images were taken at the situations of different times, varying lighting, different facial expressions (open / closed eyes, smiling / not smiling) and different facial details (glasses / no glasses). For each subject, 10 images were taken in an upright, frontal position (with tolerance for some side movement). ORL dataset is the most widely used benchmark face dataset. In this section, the size of each image is resized to 32×32 pixels, with 256 grey levels. Table I shows the classification results of different methods on ORL dataset

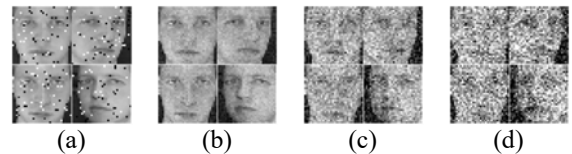


Fig. 2. ORL Samples with noises : (a)Salt&Pepper noise, (b)10std Gaussian noise, (c)30std Gaussian noise, (d)50std Gaussian noise; 10std Gaussian represents that in ORL_Train_8, the Gaussian noise with 10 standard deviation is added to the training set and test set.

with different proportions of training set and test set.

In order to verify whether the DIFL-FR has good robustness to noise, we added some typical noises (e.g., Salt & Pepper noise and Gaussian noise) in the training set and test set of ORL_Train_8 (see Fig. 2). The experimental classification results are shown in Table II, which shows that DIFL-FR is more robust to noise than the comparative methods.

In order to explore whether DIFL-FR is robust to occlusion, this section uses the same training set in ORL_Train_8, but a different test set, where an unrelated image is used to replace the randomly located region of the images to simulate the contiguous occlusion of various levels degrees from 20% to 60% (some images are shown in Fig. 3). It can be seen from the experimental results in Table III that DIFL-FR is superior to other comparison algorithms under different levels of occlusion. With 20% of pixels occluded, the accuracy of DIFL-FR achieves astonishing 99.75%, and still maintains 82.25% even when the occlusion increases as 60%. It can be concluded that DIFL-FR is not only noise-insensitive, but also has strong robustness to occlusion.

2) Extended Yale B dataset

Extended Yale B dataset consists of 2414 images with a total

of 38 individuals. For each individual around 64 near frontal images were taken under different illuminations. In this section, the size of each image is resized to 32×32 pixels, with 256 grey levels.

The experimental results are shown in Table IV. It can be seen that the classification accuracy of DIFL-FR is superior to other comparative algorithms. On EYaleB_Train_50, the DIFL-FR achieves 99.46% accuracy, and it can be concluded that DIFL-FR has strong robustness to illumination.

B. Larger-scale datasets

In this section, the proposed method DIFL-FR is evaluated on the larger-scale datasets. Specifically, the experiments are conducted on MNIST dataset [25] and Fashion-MNIST dataset [39].

1) MNIST dataset

In this section, MNIST, i.e., a handwritten digital set created by the AT&T Lab, is used for experiments. It contains 60,000 training images and 10,000 test images. The dataset is composed of handwritten digit (0 to 9) images. All digit images have been size-normalized as 28×28 pixels, with 256 grey levels.

In order to effectively evaluate the performance of the proposed method DIFL-FR, in addition to using the same comparative methods on small-scale datasets, some methods of DNNs are also concerned. This section first evaluates a very simple CNN (6-2-16-2) structure. It consists of two convolutional layers, two pooling layers and two fully-connected layers. Each convolutional layer has 6 and 12

convolutional kernels of size 5×5 respectively. The mean square error is selected as the loss function and the sigmoid function is selected as the activation function. The SGD algorithm is used to optimize the network and the number of training epochs is set as 100. This section also compares a classic CNN structure, i.e., LeNet-5 and a generative model DBM [40]. DBM is a Boltzmann machine with multiple hidden layers. Since DIFL-FR is an unsupervised deep feature learning method, we also select an unsupervised deep network, StrongNet [41], for comparison. StrongNet is an unsupervised backpropagation-free architecture with three-layer, and its tail layer is trained through a simple linear classifier. Table V shows the classification accuracies of these methods on the MNIST dataset. It can be seen that the proposed method DIFL-FR performs best in these methods.

The MNIST homepage (<http://yann.lecun.com/exdb/mnist/>) includes both the dataset itself and an extensive list of results achieved with different methods. Since this paper evaluates a DIFL-FR with two-layer of image feature learning and an output layer, its performance is compared with the two/three-layer models. The classification errors of fourteen different two/three-layer neural networks in the list ranges from 4.7% to 0.7%, and the proposed DIFL-FR error is 0.61%, which has achieved the best results in the two/three-layer models.

2) Fashion-MNIST dataset

In this section, the proposed method DIFL-FR is evaluated on the Fashion-MNIST image dataset. Fashion-MNIST is an alternative image dataset of the MNIST dataset. The dataset consists of 70,000 images of different items in 10 categories (T-

TABLE I
COMPARISON OF THE ACCURACY ON ORL DATASET WITH DIFFERENT PROPORTIONS OF TRAINING SET AND TEST SET FOR EACH METHOD (%)

Method	DIFL-FR	Raw	BlockHist	LBP	PCA	KPCA	Fisherface
ORL_Train_2	89.44±2.35	82.5±0.96	70.44±1.93	82.31±1.95	81.75±0.81	81.56±1.96	79.75±1.58
ORL_Train_5	97.7±1.04	94.3±0.76	87.2±1.82	93.9±1.56	94.1±1.08	92.7±1.15	92.9±1.14
ORL_Train_8	99.5±0.68	98±1.9	96.75±1.9	98.25±1.43	98.25±1.68	98±1.9	96.25±1.98

TABLE II
COMPARISON OF THE ACCURACY ON THE ORL_TRAIN_8 DATASET WITH DIFFERENT NOISES FOR EACH METHOD (%)

Method	DIFL-FR	Raw	BlockHist	LBP	PCA	KPCA	Fisherface
Salt&pepper	98.5±1.37	92.75±1.63	96.75±2.44	95.75±2.59	90.25±1.05	96.75±1.43	86.25±2.34
10std gaussian*	99.75±0.56	98.25±1.68	88.25±4.29	81±2.24	98±1.9	98±1.9	95.25±1.05
30std gaussian	99±3.85	94.75±2.4	56.75±2.59	19.75±4.45	94.25±2.44	96.75±1.9	88±2.27
50std gaussian	93.75±3.85	83±3.6	51±5.69	5.5±4.73	79.75±4.09	91±3.35	70.75±3.6

*: 10std Gaussian represents that in ORL_Train_8, the Gaussian noise with 10 standard deviation is added to the training set and test set.

TABLE III
COMPARISON OF ACCURACY ON THE ORL_TRAIN_8 DATASET WITH VARYING LEVELS OF OCCLUSION IN THE TEST SET FOR EACH METHOD (%)

Method	DIFL-FR	Raw	BlockHist	LBP	PCA	KPCA	Fisherface
20% Occlusion	99.75±0.56	91.25±1.77	95±3.42	97±2.59	90.5±2.09	94±1.05	81.75±2.88
40% Occlusion	98.25±2.09	55.75±4.56	86.5±4.37	80.5±1.12	53±5.2	65±4.92	41.75±2.09
60% Occlusion	82.25±6.27	14.25±3.14	74.75±4.63	34.75±1.63	15.25±3.89	29.5±2.88	13±3.81

TABLE IV
COMPARISON OF ACCURACY ON EYALEB DATASET WITH DIFFERENT PROPORTIONS OF TRAINING SET AND TEST SET FOR EACH METHOD (%)

Method	DIFL-FR	Raw	BlockHist	LBP	PCA	KPCA	Fisherface
EYaleB_Train_10	84.27±1.41	81.97±2.37	43.9±0.81	80.23±0.89	81.97±2.39	71.73±1.59	83.59±1.32
EYaleB_Train_30	99.12±0.22	95.59±0.61	71.59±0.91	95.86±0.39	95.54±0.64	90.63±1.12	81.27±1.23
EYaleB_Train_50	99.46±0.16	98.44±0.36	79.53±0.87	97.82±0.16	98.48±0.52	94.59±0.1	97.59±0.56

TABLE V
COMPARISON OF ACCURACY ON MNIST DATASET FOR EACH METHOD (%)

Traditional Method	Raw	BlockHist	LBP	PCA	KPCA	Fisherface
Accuracy	92.9	91.07	94.68	91.79	—	85.37
Deep Learning Method	CNN(6-2-16-2)	LeNet-5[25]	DBM[40]	StrongNet[41]	DIFL-FR	
Accuracy	98.8	99.05	99.05	98.9	99.39	

Note: In the comparative experiment, KPCA has no experimental result because the latitude of the construction kernel matrix is too large to exceed the memory. The experimental results of Lenet-5, DBM and StrongNet are quoted from the results of [25],[40],[41] respectively.

TABLE VI
COMPARISON OF ACCURACY ON FASHION-MNIST DATASET FOR EACH METHOD (%)

Traditional Method	Raw	BlockHist	LBP	PCA	KPCA	Fisherface
Accuracy	84.1	81.18	82.19	83.93	—	79.56
Deep Learning Method	CNN(6-2-16-2)		DNN	VGG 16	DIFL-FR	
Accuracy	89.24		88.33	93.5	91.77	

Note: In the comparison experiment, KPCA has no experimental result because the latitude of the construction kernel matrix is too large to exceed the memory.

shirts, trousers, pullovers, skirts, sneakers, etc.). The size, format, and training set/test set partitioning of Fashion-MNIST are identical to the MNIST.

Similarly, on the Fashion-MNIST dataset, in addition to the same comparative algorithms aforementioned, a DNN with three hidden layers was also evaluated where the hidden layer structure is 256-128-100. We select loss function as the mean square error, the activation function as the tanh function, the optimization algorithm as the SGD, and the number of epochs as 100. In addition, a CNN framework with more layers, i.e., VGG 16 is compared. In the experiment, the standard structure of VGG 16 is adopted, where the cross-entropy loss, ReLU activation function, Adam optimization algorithm are adopted, and the number of epochs is set as 100. Table VI shows the accuracies of these methods. DIFL-FR is superior to the traditional feature extraction methods and the two/three-layer neural networks, but a little inferior to VGG 16. However, the proposed method is more interpretable than VGG 16 due to the introduction of rules in it. Moreover, the performance of the proposed method can be further enhanced when the improved criterion, such as semi-supervised objective is adopted to learning the parameters of fuzzy rules.

For the Effectiveness Analysis of Fuzzy System Feature Extraction Module in DIFL-FR, please see Part F of the *Supplementary Materials* section. Moreover, a more comprehensive parameters analysis of the proposed DIFL-FR method is also presented in Part G of the *Supplementary Materials* section.

V. CONCLUSIONS

The paper proposes a deep image feature learning method with fuzzy rules which is a stacked feature learning structure based on TSK-FS. The experimental results show that the proposed method is superior to traditional hand-crafted feature extraction method. Compared with DNNs that tend to over-fit when there are few data in training sets, the proposed method achieves satisfactory results on small datasets. On the larger-scale datasets, the results of the proposed method are comparable to those of deep neural networks. In particular, feature learning with fuzzy rules in DIFL-FR not only provides

the ability of nonlinear feature learning to enhance the learning ability, but also brings good interpretability.

In the future, we will make in-depth research into deep image feature learning based on TSK-FS from the following aspects. In the proposed DIFL-FR, the depth of the network structure will be explored to further increase the capacity of the model. Furthermore, this paper uses PCA to preserve the data geometric properties in the feature learning phase of each layer, which can only preserve the global structure of the data and is under the unsupervised settings. In the future study, we will try to use techniques that can preserve the local structure of the data and add supervised learning strategies to further improve the performance.

REFERENCES

- [1] N. Dalal and B. Triggs, "Histograms of Oriented Gradients for Human Detection," in *2005 IEEE Computer Society Conference on Computer Vision and Pattern Recognition (CVPR'05)*, San Diego, CA, USA, Jun. 2005, pp. 886–893.
- [2] T. Ojala, M. Pietikainen, and T. Maenpaa, "Multiresolution gray-scale and rotation invariant texture classification with local binary patterns," *IEEE transactions on Pattern Anal. Machine Intell.*, vol. 24, no. 7, pp. 971–987, 2002.
- [3] F.-F. Li and P. Perona, "A Bayesian Hierarchical Model for Learning Natural Scene Categories," in *2005 IEEE Computer Society Conference on Computer Vision and Pattern Recognition (CVPR'05)*, San Diego, CA, USA, Jun. 2005, pp. 524–531.
- [4] L. Liu, L. Wang, and X. Liu, "In defense of soft-assignment coding," in *2011 International Conference on Computer Vision, Barcelona, Spain, Nov. 2011 - Nov. 2011*, pp. 2486–2493.
- [5] J. Philbin, O. Chum, M. Isard, J. Sivic, and A. Zisserman, "Lost in quantization: Improving particular object retrieval in large scale image databases," in *2008 IEEE Conference on Computer Vision and Pattern Recognition*, Anchorage, AK, USA, Jun. 2008 - Jun. 2008, pp. 1–8.
- [6] J. Wang et al., "Locality-constrained Linear Coding for image classification," in *2010 IEEE Computer Society Conference on Computer Vision and Pattern Recognition*, San Francisco, CA, USA, Jun. 2010 - Jun. 2010, pp. 3360–3367.
- [7] J. Yang, K. Yu, Y. Gong, and T. Huang, "Linear spatial pyramid matching using sparse coding for image classification," in *2009 IEEE Conference on Computer Vision and Pattern Recognition*, Miami, FL, Jun. 2009 - Jun. 2009, pp. 1794–1801.

- [8] A. Gersho and B. Ramamurthi, "Image coding using vector quantization," in *ICASSP '82. IEEE International Conference on Acoustics, Speech, and Signal Processing*, Paris, France, May. 1982, pp. 428–431.
- [9] G. J. Garateguy, G. R. Arce, D. L. Lau, and O. P. Villarreal, "QR images: optimized image embedding in QR codes," *IEEE transactions on image processing*, vol. 23, no. 7, pp. 2842–2853, 2014.
- [10] Q. Zhang and B. Li, "Discriminative K-SVD for dictionary learning in face recognition," in *2010 IEEE Computer Society Conference on Computer Vision and Pattern Recognition*, San Francisco, CA, USA, Jun. 2010 - Jun. 2010, pp. 2691–2698.
- [11] J. Yang, J. Wright, T. S. Huang, and Y. Ma, "Image super-resolution via sparse representation," *IEEE transactions on image processing*, vol. 19, no. 11, pp. 2861–2873, 2010.
- [12] M. Turk and A. Pentland, "Eigenfaces for recognition," *Journal of Cognitive Neuroscience*, vol. 3, no. 1, pp. 71–86, 1991.
- [13] S. Wold, K. Esbensen, and P. Geladi, "Principal component analysis," *Chemometrics and Intelligent Laboratory Systems*, vol. 2, no. 1-3, pp. 37–52, 1987.
- [14] P. N. Belhumeur, J. P. Hespanha, and D. J. Kriegman, "Eigenfaces vs. Fisherfaces: Recognition using class specific linear projection," in *Lecture Notes in Computer Science, Computer Vision — ECCV '96*, G. Goos, J. Hartmanis, J. van Leeuwen, B. Buxton, and R. Cipolla, Eds., Berlin, Heidelberg: Springer Berlin Heidelberg, 1996, pp. 43–58.
- [15] J. Lu, K. N. Plataniotis, and A. N. Venetsanopoulos, "Face recognition using LDA-based algorithms," *IEEE transactions on neural networks*, vol. 14, no. 1, pp. 195–200, 2003.
- [16] Y. Bengio and O. Delalleau, "On the Expressive Power of Deep Architectures," in *Lecture Notes in Computer Science, Algorithmic Learning Theory*, J. Kivinen, C. Szepesvári, E. Ukkonen, and T. Zeugmann, Eds., Berlin, Heidelberg: Springer Berlin Heidelberg, 2011, pp. 18–36.
- [17] G. E. Hinton, S. Osindero, and Y.-W. Teh, "A fast learning algorithm for deep belief nets," *Neural computation*, vol. 18, no. 7, pp. 1527–1554, 2006.
- [18] A. Krizhevsky, I. Sutskever, and G. E. Hinton, "ImageNet classification with deep convolutional neural networks," *Commun. ACM*, vol. 60, no. 6, pp. 84–90, 2017.
- [19] Y. Bengio, A. Courville, and P. Vincent, "Representation learning: a review and new perspectives," *IEEE transactions on Pattern Anal. Machine Intell.*, vol. 35, no. 8, pp. 1798–1828, 2013.
- [20] Hecht-Nielsen, "Theory of the backpropagation neural network," in *International Joint Conference on Neural Networks, Washington, DC, USA, Jun. 1990 - Jun. 1990*, 593-605 vol.1.
- [21] L. Bottou, "Large-Scale Machine Learning with Stochastic Gradient Descent," in *Proceedings of COMPSTAT'2010*, Y. Lechevallier and G. Saporta, Eds., Heidelberg: Physica-Verlag HD, 2010, pp. 177–186.
- [22] R. Alcalá, J. Alcalá-Fdez, J. Casillas, O. Cordón, and F. Herrera, "Local identification of prototypes for genetic learning of accurate TSK fuzzy rule-based systems," *Int. J. Intell. Syst.*, vol. 22, no. 9, pp. 909–941, 2007.
- [23] Y. Zhang, H. Ishibuchi, and S. Wang, "Deep Takagi–Sugeno–Kang fuzzy classifier with shared linguistic fuzzy rules," *IEEE Trans. Fuzzy Syst.*, vol. 26, no. 3, pp. 1535–1549, 2018.
- [24] P.-C. Chang and C.-H. Liu, "A TSK type fuzzy rule based system for stock price prediction," *Expert Systems with Applications*, vol. 34, no. 1, pp. 135–144, 2008.
- [25] Y. Lecun, L. Bottou, Y. Bengio, and P. Haffner, "Gradient-based learning applied to document recognition," *Proc. IEEE*, vol. 86, no. 11, pp. 2278–2324, 1998.
- [26] C. Szegedy et al., "Going deeper with convolutions," in *2015 IEEE Conference on Computer Vision and Pattern Recognition (CVPR)*, Boston, MA, USA, Jun. 2015 - Jun. 2015, pp. 1–9.
- [27] K. Simonyan and A. Zisserman, "Very Deep Convolutional Networks for Large-Scale Image Recognition," *Computer Science*, 2014.
- [28] B. Zhou, A. Khosla, A. Lapedriza, A. Oliva, and A. Torralba, "Learning Deep Features for Discriminative Localization," in *2016 IEEE Conference on Computer Vision and Pattern Recognition (CVPR)*, Las Vegas, NV, USA, Jun. 2016 - Jun. 2016, pp. 2921–2929.
- [29] T. Takagi and M. Sugeno, "Fuzzy identification of systems and its applications to modeling and control," *IEEE transactions on Syst., Man, Cybern.*, vol. SMC-15, no. 1, pp. 116–132, 1985.
- [30] H. Carter, D. Dubois, and H. Prade, "Fuzzy Sets and Systems -- Theory and Applications," *The Journal of the Operational Research Society*, vol. 33, no. 2, p. 198, 1982.
- [31] M. Sugeno and G.T. Kang, "Structure identification of fuzzy model," *Fuzzy Sets and Systems*, vol. 28, no. 1, pp. 15–33, 1988.
- [32] J. C. Bezdek, *Pattern Recognition with Fuzzy Objective Function Algorithms*. Boston, MA: Springer US, 1981.
- [33] A. Blum and T. Mitchell, "Combining labeled and unlabeled data with co-training," in *Proceedings of the eleventh annual conference on Computational learning theory - COLT' 98*, Madison, Wisconsin, United States, 1998, pp. 92–100.
- [34] T. Su and J. G. Dy, "In search of deterministic methods for initializing K-means and Gaussian mixture clustering," *Intelligent Data Analysis*, vol. 11, no. 4, pp. 319–338, 2006.
- [35] C.-C. Chang and C.-J. Lin, "LIBSVM," *ACM transactions on Intell. Syst. Technol.*, vol. 2, no. 3, pp. 1–27, 2011.
- [36] D. Cai, X. He, J. Han, and H.-J. Zhang, "Orthogonal Laplacianfaces for Face Recognition," *IEEE transactions on Image Process.*, vol. 15, no. 11, pp. 3608–3614, 2006.
- [37] D. Cai, X. He, and J. Han, "Spectral Regression for Efficient Regularized Subspace Learning," in *2007 IEEE 11th International Conference on Computer Vision*, Rio de Janeiro, Brazil, Oct. 2007 - Oct. 2007, pp. 1–8.
- [38] X. He, S. Yan, Y. Hu, P. Niyogi, and H.-J. Zhang, "Face recognition using laplacianfaces," *IEEE transactions on Pattern Anal. Machine Intell.*, vol. 27, no. 3, pp. 328–340, 2005.
- [39] H. Xiao, K. Rasul, and R. Vollgraf, "Fashion-MNIST: a Novel Image Dataset for Benchmarking Machine Learning Algorithms," 2017.
- [40] R. Salakhutdinov and G. Hinton, "An efficient learning procedure for deep Boltzmann machines," *Neural computation*, vol. 24, no. 8, pp. 1967–2006, 2012.
- [41] M. Albonico et al., "StrongNet: An International Network to Improve Diagnostics and Access to Treatment for Strongyloidiasis Control," *Plos Neglected Tropical Diseases*, vol. 10, no. 9, e0004898, 2016.

Supplementary Materials

Part A: Some additional illustrations of DIFL-FR

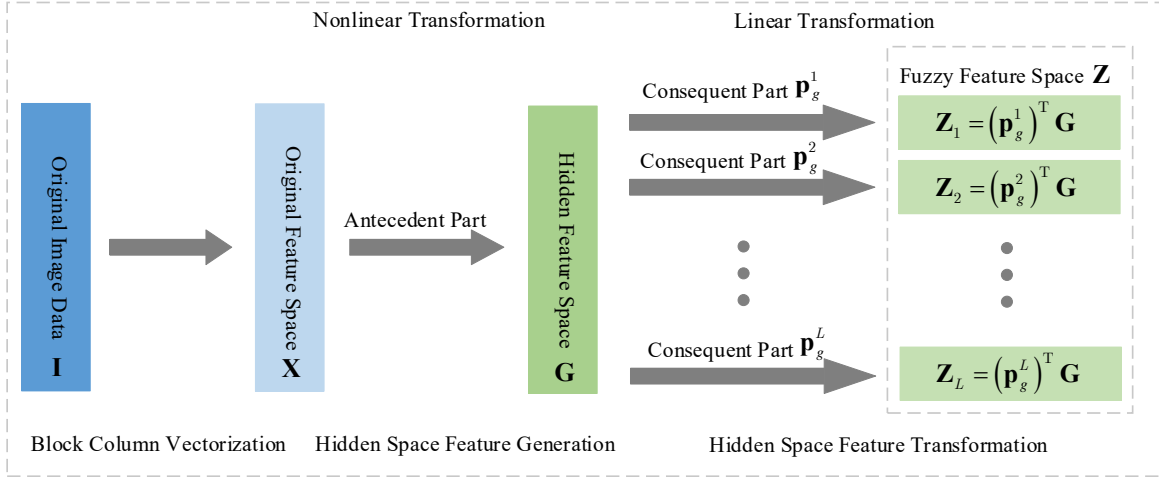


Fig. S1 The flowchart of TSK-FS image feature learning

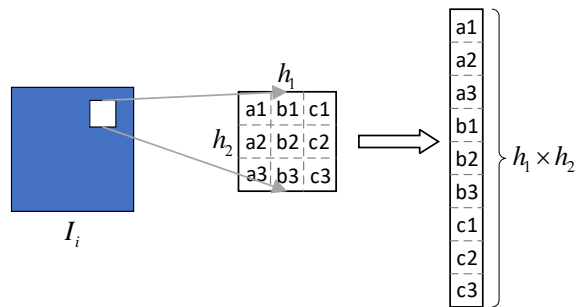


Fig. S2 The illustration of block column vectorization

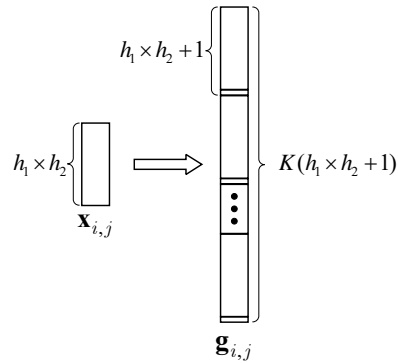


Fig. S3 The illustration of hidden space feature generation based on TSK-FS

Part B: Details of Var-Part

The core task of estimating the antecedent parameters of TSK-FS using the Var-Part algorithm is to cluster the training input data sets \mathbf{X} to obtain the K clusters. The process is as follows. First, all samples are treated as a cluster, which is the initialized set of the currently obtained cluster. Then choose the next cluster to partition by selecting the cluster with the largest within-cluster sum-squared-error. After one partition, two clusters are obtained instead of the partitioned clusters. And repeat the above process until K clusters are produced. The process of partitioning a cluster is as follows: For the current cluster C_j to partition, it is to firstly compute the variance in each dimension and find the dimension with the largest variance, such as d_p . Then, let x_{ip} denote the value of example \mathbf{x}_i in feature d_p , μ_{jp} denote the mean of C_j in feature d_p , and divide C_j into two sub-clusters C_{j1} and C_{j2} , according to the following rule: If x_{ip} is less than or equal to μ_{jp} , assign \mathbf{x}_i to C_{j1} ; otherwise, assign \mathbf{x}_i to C_{j2} .

The K cluster centers calculated by the deterministic clustering algorithm Var-Part can be represented as a clustering center matrix \mathbf{C} . Once the clustering center matrix \mathbf{C} is known, the kernel width matrix \mathbf{D} can be calculated with (A1).

$$D_p^k = \sum_{i=1}^N (x_{ip} - C_p^k)^2 \tag{A 1}$$

where $k = 1, 2, \dots, K$ and K is the number of fuzzy rules, d is the dimension of the examples and $p = 1, 2, \dots, d$. (A2.1) is used for calculating the kernel widths of the data, where x_{ip} represents the value of example in feature d_p . Furthermore, the kernel width for each dimension is scaled to the range [1, 10], which is a reasonable range based on extensive experiments.

Part C: Details of multi-output TSK-FS

In order to extract different features form images, TSK-FS image feature learning implements feature extraction through the multi-output TSK-FS. The main difference between the multi-output TSK-FS and the single-output TSK-FS is that there are multiple-group consequent parameters in the multi-output TSK-FS. Therefore, multiple outputs can be obtained from different groups of consequent parameters. TSK-FS image feature learning uses these multiple outputs to extract different features from images.

The fuzzy rule of TSK-FS with L outputs can be represented as (A2):

Rule k

IF: x_1 is $A_1^k \wedge x_2$ is $A_2^k \wedge \dots \wedge x_d$ is A_d^k ,

THEN: $f_1^k(\mathbf{x}) = p_{0,1}^k + p_{1,1}^k x_1 + \dots + p_{d,1}^k x_d$,

$f_2^k(\mathbf{x}) = p_{0,2}^k + p_{1,2}^k x_1 + \dots + p_{d,2}^k x_d$,

\vdots

$f_L^k(\mathbf{x}) = p_{0,L}^k + p_{1,L}^k x_1 + \dots + p_{d,L}^k x_d$,

$k = 1, 2, \dots, K$.

(A 2)

The l -th ($1 \leq l \leq L$) output of the multi-output TSK-FS can be represented as (A3):

$$y_l = \sum_{k=1}^K \tilde{\mu}^k(\mathbf{x}) f_l^k(\mathbf{x})$$

(A 3)

Just like the single-output TSK-FS, d is the dimension of the samples, A_i^k is a fuzzy set in the i -th input feature for the k -th rule, and \wedge is a fuzzy conjunction operator. The process of generating the antecedent parameters is the same as that of the single-output TSK-FS. K represents the number of rules of the multi-output TSK-FS. The main distinction between the multi-output TSK-FS and the single-output TSK-FS in (A2) is that there are L groups of consequent parameters in the multi-output TSK-FS, corresponding to L output. $f_l^k(\mathbf{x})$ represents the l -th output of the k -th rule in the multi-output TSK-FS.

Let

$$\mathbf{p}_l^k = (p_{0,l}^k, p_{1,l}^k, \dots, p_{d,l}^k)^T \in R^{(d+1) \times 1}$$

(A 4)

$$\mathbf{p}_g^l = \left[(\mathbf{p}_l^1)^T, (\mathbf{p}_l^2)^T, \dots, (\mathbf{p}_l^K)^T \right]^T \in R^{K(d+1) \times 1}$$

(A 5)

$$\mathbf{P} = [\mathbf{p}_g^1, \mathbf{p}_g^2, \dots, \mathbf{p}_g^L] \in R^{K(d+1) \times L}$$

(A 6)

With \mathbf{x}_g defined as in (2.3a) -(2.3c) in the main text, the final output of the multi-output can be represented as (1.3d).

$$\mathbf{y} = [y_1, \dots, y_L] = \mathbf{P}^T \mathbf{x}_g$$

(1.3 d)

Here \mathbf{P} in (A5) denotes the matrix of consequent parameters for the L -dimensional output TSK-FS.

Part D: Algorithm description of DIFL-FR

TABLE S1
DESCRIPTION OF DIFL-FR ALGORITHM

Algorithm: DIFL-FR
Input: Image dataset $\mathbf{I} = \{\mathbf{I}_i\}_{i=1}^N$; the patch size for each pixel $h_1 \times h_2$; the number of the layers for TSK-FS image feature learning S ; the number of fuzzy rules for each layer TSK-FS K_s ; the number of consequent parameters groups for each layer TSK-FS image feature learning L_s ; overlap ratio of the block-wise histogram Cr (default is 0.5).
Output: New feature data \mathbf{F} extracted for the image.
Procedure DIFL-FR:
1): The first layer TSK-FS image feature learning
1: Transform the original image dataset matrix \mathbf{I} to column vector matrix \mathbf{x} .
2: Calculate the antecedent parameters \mathbf{C} and \mathbf{D} .
3: Calculate the hidden space data matrix \mathbf{G} using \mathbf{C} , \mathbf{D} and \mathbf{x} .
4: Calculate the consequent parameters \mathbf{P} .
5: Generate data \mathbf{Z}^1 for the new feature space.
6: Reconstruct the data \mathbf{Z}^1 for the new feature space into the image feature matrix \mathbf{I}^1 .
2): The second to the Sth layers TSK-FS image feature learning
7: For $s=2:S$ do
8: Transform the $s-1$ th feature image matrix \mathbf{I}^{s-1} to column vector matrix \mathbf{X}^s .
9: Transform \mathbf{X}^s to the hidden space data matrix \mathbf{G}^s based on steps 2 and 3 in 1).
10: Calculate the consequent parameters \mathbf{P}^s based on step 4 in 1).
11: Generate data \mathbf{Z}^s for the new feature space.
12: Reconstruct the data \mathbf{Z}^s for the new feature space into the image feature matrix \mathbf{I}^s .
13: end for
3): Output layer
14: Transform the feature matrix \mathbf{I}^S to integer-valued feature image matrix \mathbf{T} .
15: Transform \mathbf{T} to the feature matrix \mathbf{F} using a block-wise histogram operator.

Part E: Description of face datasets partition

TABLE S2
DESCRIPTION OF FACE DATASETS PARTITION

Raw dataset	Divided dataset	Description of the specific division
ORL	ORL_Train_2	A random subset with 2 images per individual was taken to form the training set, and the rest of the database was considered to be the testing set. The size of the divided training set/testing set is 80/320.
	ORL_Train_5	A random subset with 5 images per individual was taken to form the training set, and the rest of the database was considered to be the testing set. The size of the divided training set/testing set is 200/200.
	ORL_Train_8	A random subset with 8 images per individual was taken to form the training set, and the rest of the database was considered to be the testing set. The size of the divided training set/testing set is 320/80.
Extended Yale B	EYaleB_Train_10	A random subset with 10 images per individual was taken to form the training set, and the rest of the database was considered to be the testing set. The size of the divided training set/testing set is 380/2034.
	EYaleB_Train_30	A random subset with 30 images per individual was taken to form the training set, and the rest of the database was considered to be the testing set. The size of the divided training set/testing set is 1140/1274.
	EYaleB_Train_50	A random subset with 50 images per individual was taken to form the training set, and the rest of the database was considered to be the testing set. The size of the divided training set/testing set is 1900/514.

Part F: Effectiveness Analysis of Fuzzy System Feature Extraction Module in DIFL-FR

In order to verify the effectiveness of the feature learning module based on TSK-FS in the proposed method DIFL-FR, the following comparison is conducted between two methods. The first method is named as DIFL-FR+SVM, for which the multi-layer TSK-FS feature learning is used before the block-wise histograms feature extraction in the output layer. The second method is named as BlockHist+SVM, for which only the block-wise histogram is used for feature extraction on the original image. These two feature extraction methods are then combined with linear SVM to classify different datasets. Fig. S4 shows that the accuracy of DIFL-FR+SVM on four different datasets is much higher than the accuracy of BlockHist+SVM. Therefore, it can be concluded that the TSK-FS feature learning module in DIFL-FR significantly improves the feature learning ability.

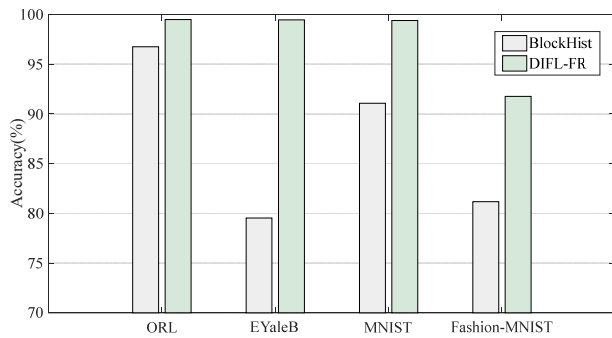


Fig. S4 Comparison of accuracy between block histogram and DIFL-FR

Part G: Parameters Analysis of DIFL-FR

Three parameters of DIFL-FR are analyzed to study the sensitivity of the proposed method to these parameters, i.e., the number of layers of TSK-FS, the number of fuzzy rules of each layer of TSK-FS, and the number of groups of consequent part. The small-scale face datasets (i.e., ORL dataset and Extended Yale B dataset) and the larger-scale datasets (i.e., MNIST dataset and Fashion-MNIST dataset) are used for analyzing the parameters. ORL_Train_8 and EYaleB_Train_50 are selected from ORL dataset and Extended Yale B dataset respectively.

1) *Impact of The Number of The Layers in DIFL-FR*

In order to study the impact of the number of layers on the method, this section uses DIFL-FR with one layer (DIFL-FR_1), two layers (DIFL-FR_2), and three layers (DIFL-FR_3) for comparison. Each model is optimized by grid search on all parameters to obtain the best classification accuracy. The experimental results are shown in Fig. S5. Fig. S5 illustrates that the accuracy of the DIFL-FR with two layers shows great superiority compared with only one-layer structure, and the accuracy of the three-layer structure is almost the same with that of the two-layer structure, sometimes even worse. Therefore, it is reasonable to select the two-layer structure in the previous experiments.

2) *Impact of The Number of Fuzzy Rules*

In order to study the impact of the number of fuzzy rules on the performance of the two-layer DIFL-FR, the number of fuzzy

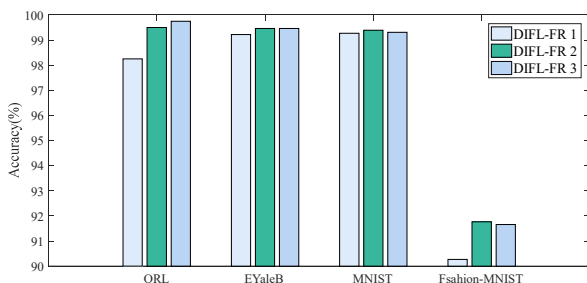


Fig. S5 Impact of the number of the TSK-FS layers in DIFL-FR on classification performance.

rules is set from 2 to 15 with the interval as 1 in the experiments and the number of rules for each layer is set to be the same. The other parameters are fixed, i.e., the block size of each pixel point is set as 7×7 , and the number of groups of consequent parameters with each layer is set as 8. Fig. S6 shows that the promising accuracy are achieved on these datasets when the number of rules is 2 or 3. As the number of rules increases, the accuracy decreases with fluctuations. For high-dimensional image datasets, the number of parameters of the model increases rapidly with the increase of the number of fuzzy rules. Therefore, it can be concluded from Fig. S6 that good performance can be obtained with only a few fuzzy rules on the high-dimensional datasets.

3) *Impact of The Number of Groups of The Consequent Part*

In order to study the impact of the number of groups of the consequent part on the performance of the two-layer DIFL-FR, the number of groups of the consequent part is set from 4 to 15 with the interval as 1 in the experiments and the number of rules for each layer is set to be the same. The other parameters are fixed, i.e., the block size of each pixel point is set as 7×7 , and the number of fuzzy rules with each layer is set as 3. Fig. S7 shows that the accuracy of these datasets increases with the increasing number of groups of the consequent part. For two small-scale datasets, the accuracy tends to be stable when the number is larger than 8.

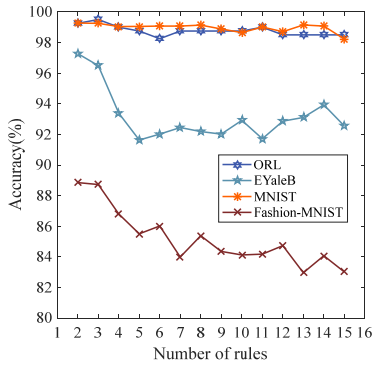


Fig. S6 Impact of the number of fuzzy rules M in DIFL-FR on classification performance

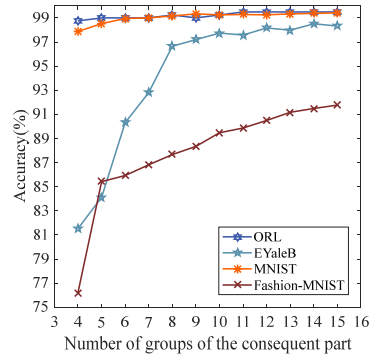


Fig. S7 Impact of the number of groups of the consequent part for TSK-FS in DIFL-FR on classification performance